Chaos and period-adding; an experimental verification of the grazing bifurcation normal form

Petri T. Piiroinen* Lawrence N. Virgin† Alan R. Champneys*

November 20, 2003

Abstract

Experimental results are presented for a single degree of freedom horizontally excited pendulum that is allowed to impact with a rigid stop at a fixed angle $\hat{\theta}$ to the vertical. By inclining the apparatus, the pendulum is allowed to swing in an effectively reduced gravity, so that for each fixed $\hat{\theta}$ less than a critical value, a forcing frequency is found such that a period-one limit cycle motion just grazes with the stop. Experimental measurements show the immediate onset of chaotic dynamics and a period-adding cascade for slightly higher frequencies. These results are compared with a numerical simulation and continuation of solutions to a mathematical model of the system, which shows the same qualitative effects. From the model, the theory of discontinuity mappings due to Nordmark is applied to derive the coefficients of the square-root normal form map of the grazing bifurcation for this system. The grazing periodic orbit and its linearisation are found using a novel numerical continuation method for hybrid systems. From this, the normal-form coefficients are computed, which in this case imply that a jump to chaos and period-adding cascade occurs. Excellent quantitative agreement is found between the model simulation and the map, even over wide parameter ranges. Qualitatively, both accurately predict the experimental results, and after a slight change in the effective damping value, a striking quantitative agreement is found too.

1 Introduction

Many mechanical systems exhibiting sustained finite-amplitude oscillatory motion do so because of some kind of discontinuity or non-smoothness. Effects of this nature include vibro-impact, rattling due to freeplay or backlash, stick-slip motion due to friction as well as the discrete or delayed interaction with a control system, see for example [52, 5, 46, 2, 1, 17] to name but a few of the vast number of references on this subject. There are also analogues in electronics (e.g. [11]) biology (e.g. [30]) and almost all other areas in which dynamical systems arise. Such systems have been found to show a remarkable variety of different long-time behaviour, such as periodic, quasi-periodic and chaotic motions and to undergo all the bifurcations that may occur for smooth systems (fold, Hopf, period-doubling etc.). They also undergo bifurcations that are unique to non-smooth systems (so called C-bifurcations [16, 14]) which occur when an ω-limit set approaches a discontinuity surface within the

*Bristol Center for Applied Nonlinear Mathematics, Department of Engineering Mathematics, University of Bristol, Bristol BS8 1TR, United Kingdom

†Department of Mechanical Engineering, Duke University, Durham, NC 27708-0300, USA

phase space. Such transitions include border-collision bifurcation in maps [16, 38], boundary transition of equilibria in flows [31, 30] or the grazing [35, 9], sliding [15], chattering [6] or corner-collision [13] of a periodic orbit. In this paper we shall focus on the bifurcation caused by *grazing* (zero-velocity impact) of a periodic orbit with a hard constraint.

There are basically two different ways to model impacts in mechanics (see e.g. [50, 42, 57]); either as elastic, with the contact between the bodies taking a finite time, or as completely rigid and instantaneous. In the former case there is a small penetration into the unilateral stop and typically the propagation of shock waves, while in the latter one assumes that the velocity is immediately reversed at impact with some impulsive loss of energy (a restitution law). We shall adopt the second approach here, which has been shown to be a good model for point contacts in the absence of friction. Hence one typically arrives at low-degree-of-freedom smooth (even linear) dynamical models between impacts, with a discontinuity in velocity whenever the system hits some hard constraint in configuration space. Examples of such impact-oscillator systems arise in practice as models of bouncing balls [22], rattling gears [26], colliding boiler tubes [21], car suspensions [25], Braille printers [24, 10], percussive drilling [28, 3], and walking machines (including the human walking apparatus) [32, 43, 45].

It has been known since the pioneering work of Peterka [40, 41], who studied a simple harmonic oscillator with sinusoidal forcing and impact, that low velocity impact can have a profound implication for the dynamics. Shaw & Holmes [47] showed that such grazing events in impact oscillators can lead to the disappearance of stable periodic motion, and Whiston [55, 54] showed the onset of chaotic motions of low velocity impacts which can have a characteristic *fingered* appearance (see also Thompson & Ghaffari [51] and Fig. 11 below). The key idea is that Poincaré maps associated with grazing have infinite local stretching due to a square-root singularity, which has strong implications on the geometry of phase space [56, 7].

As with smooth dynamical systems in order to explain this and related behaviour, it is desirable to derive *normal forms* that enable all possible long term dynamics at nearby parameter values to be described. The same philosophy applies to non-smooth bifurcations such as that brought about by grazing. The key concept here is that of the *discontinuity mapping* introduced by Nordmark [35, 36, 18]. This allows the analytical derivation of the appropriate Poincaré map directly from the flow, given only information about the grazing periodic orbit and its linearisation (see Sect. 5 below). The resulting mappings have a square-root singularity and their dynamics can be classified using simple iterative techniques [8, 37]. Depending on the coefficients of the normal form, various scenarios are possible. These include the sudden birth or destruction of stable periodic motion, the sudden jump to chaos (with fingered attractors), and so called *period-adding*, where an infinite number of periodic orbits appear which become stable in successive parameter intervals with the periodicity increased (decreased) by one each time. These intervals may occur as *windows* interspersed within the main region of chaos, and should be contrasted with the situation for smooth unimodal maps where the periodicity of the windows obeys the usual Sarkovskii ordering [12].

There is significant experimental evidence for complex dynamics in impact oscillator systems. See for example [4, 49, 20, 53]. Some of the most convincing experimental verification of the dynamics of a single-degree-of-freedom impact oscillator occurs in the work of Oestreich *et al* [39], where excellent agreement is found

between experimental and numerical one-parameter bifurcation diagrams. Within the parameter sweep are values where already impacting orbits undergo further (internal) grazing with the stop. However we are not aware of any work on experimental verification of a grazing bifurcation where the pre-grazing orbit is a period-one non-impacting limit cycle. It is precisely this situation we investigate here, and in addition to comparison with numerics, we shall also evaluate the normal form for the grazing to explain the details of the dynamics observed in the experiment.

The rest of this paper is organized as follows. In Sect. 2 the experimental setup is introduced and its results are presented. Section 3 introduces the equations of motion for the impacting mechanism and introduces and in Sect. 4 numerical techniques used to simulate and analyze periodic solutions are introduced. In Sect. 5 some aspects of grazing bifurcation theory are introduced, culminating in the derivation of the discontinuity map for the specific problem analysed here. Section 6 presents results of the numerics and analysis and compares them with the experiment, including a brief discussion on overcoming experimental uncertainty. Finally, Sect. 7 draws conclusions.

2 Experiments

The experimental results described here were obtained using the apparatus used in the earlier results of Bayly, Virgin and Slade [4, 48]. Those works focused on chattering solutions, and the careful extraction of data from recording of the time between impacts. Here, a novel adaptation of the apparatus is considered which allows the variation of the position of the impacting stop in order to specifically investigate grazing.

2.1 The experimental system

A simple rigid-arm pendulum that strikes a vertical impact surface is an easily realized single-degree-of-freedom discontinuous mechanical oscillator [4]. By horizontally shaking the supporting pivot of the pendulum a variety of dynamic behavior can be observed including chaos. However, with the impact barrier located at static equilibrium (see Fig. 1) the velocity of impact tends to be relatively high and thus grazing bifurcations of the fundamental *period-one* (i.e. with the same period as the forcing) do not typically occur. But, by inclining the angle at which the pendulum mass strikes the barrier, it is possible to observe the subtle transition between non-contacting and contacting dynamic behavior. If the impact surface is placed sufficiently far from static equilibrium (i.e., to the left of equilibrium) and the forcing is relatively low, then impact will not take place. For intermediate angles of impact, as a parameter is changed however, contact is initiated, and it is the interesting behavior associated with this discrete transition that is the focus of the current study.

The pendulum is constructed using a relatively light aluminium arm of length 305 mm and a steel mass of diameter 25.4 mm attached at the end. The pivot of the pendulum consists of low-friction bearings and a rotational potentiometer measures the angle $\theta(t)$. The assembly is mounted on a Scotch-yoke driven shake table which imparts a harmonic base displacement. Due to speed limitations of the forcing mechanism the assembly was inclined at an angle of $\Theta = 1.33$ radians (out of plane, see the right-hand side of Fig. 1) in order to change the effect of gravity,

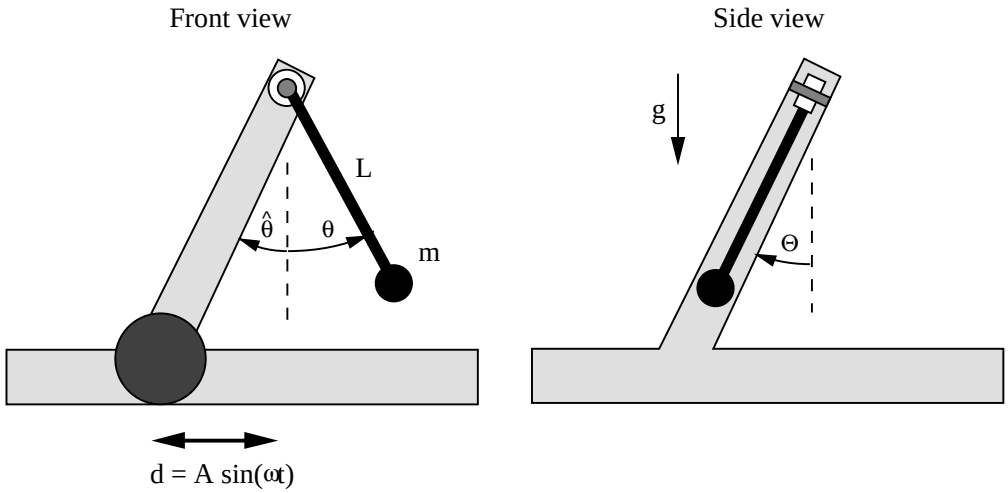

Figure 1: *Schematic of the pendulum/impact barrier assembly.*

i.e., $g_e = 0.24g$, and thus reduce the natural frequency of the system. The measured natural frequency indicated that the pendulum arm and end mass resulted in an effective length of an ideal pendulum of $L = 225$ mm. The forcing amplitude A was chosen as 50.8 mm (centre to peak) and this was held fixed for all the experiments. The angle of contact with the impact barrier $\hat{\theta}$ and the forcing frequency ω were used as the primary control parameters: the former fixed at discrete values at intervals of 10° and the latter varied statically by small amounts. The forcing mechanism allowed a discrete (Poincaré) sampling of the response, i.e., every time the flywheel of the Scotch-yoke passed through a certain phase, the angle of the pendulum θ at that specific instant of time was extracted. At each new parameter value data was recorded, with a rotational potentiometer attached to the pivot of the pendulum, only after a sufficient amount of time for transients to decay.

A crucial issue in modelling many mechanical systems is the estimation of the amount of damping. Damping in this system is primarily due to the coefficient of restitution at impact, but may also arise from a number of other factors, such as coulomb friction in the bearing and viscous air drag. In order to estimate the overall damping, a simple logarithmic decrement method was used to the response when $\hat{\theta} = 0$ and no forcing was present. Successive peak amplitudes A_k, $k = 1, 2, \ldots$, were recorded and an overall damping factor D recorded according to the standard formula

$$D = \frac{1}{4\pi\hat{k}} \ln\left(\frac{A_k}{A_{k+\hat{k}}}\right), \tag{1}$$

where $\hat{k}$ is a positive integer. The effect of external noise may be minimized by choosing amplitudes a number of impacts apart, i.e. by choosing $\hat{k} > 1$. A value for D was obtained by averaging over several runs, from which it was estimated that $D = 0.07$, that is 7% of crtical damping.

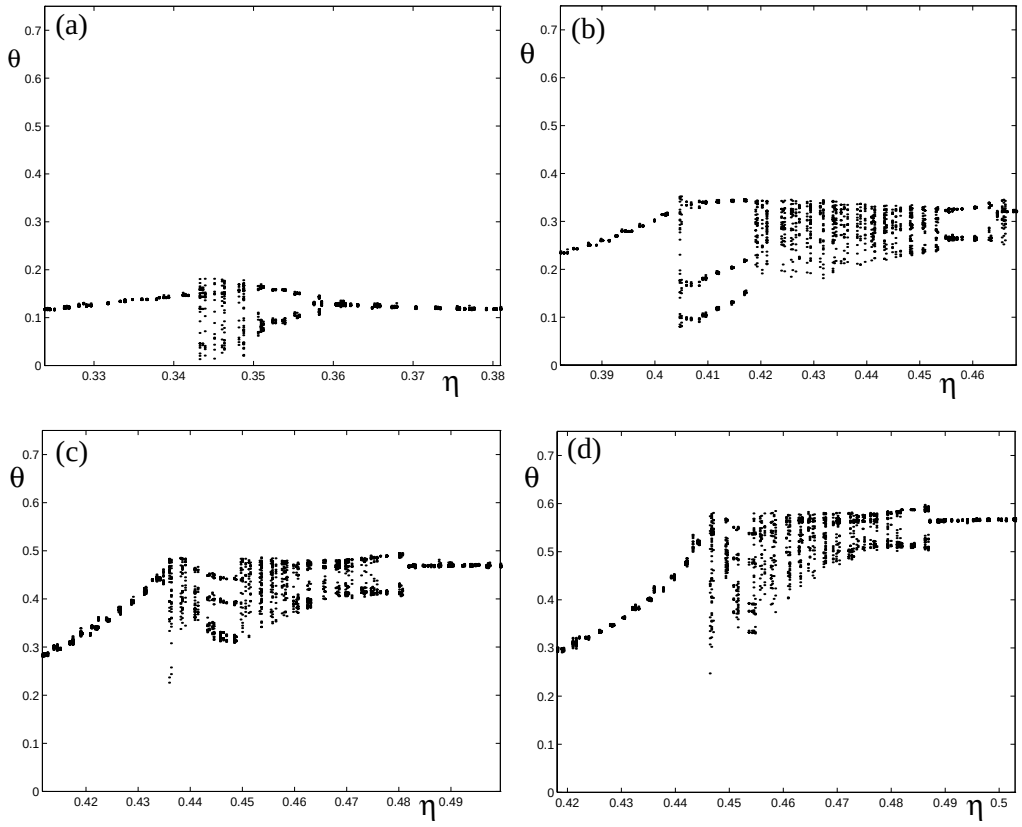

Figure 2: *Experimental bifurcation diagrams in which the response is sampled once during a forcing cycle (at an arbitrary but consistent phase p). (a)* $\hat{\theta} = 10°$*, (b)* $\hat{\theta} = 20°$*, (c)* $\hat{\theta} = 30°$*, (d)* $\hat{\theta} = 40°$*.*

2.2 Results

Figures 2 and 3 summarize, for four different values of $\hat{\theta}$, the response of the pendulum when the forcing frequency is gradually increased through the range of primary resonance. Forcing frequency is measured as a ratio η to the natural frequency of an impacting pendulum (see (3) below), so that the primary resonance is at $\eta = 1/2$.

The angle of the stop was varied in intervals of 10° from $\hat{\theta} = 0°$. The case $\hat{\theta} = 0°$ was thoroughly described in [4]. Complex dynamics occurs, but grazing bifurcations do not play a major role, so we do not consider this case further here. For each $\hat{\theta}$-value between 10° and 40° inclusive, a critical forcing frequency $\eta = \eta_c$ was found below which a period-one limit cycle exists which does not impact. At η_c this limit cycle just grazes with the stop, and impacting motion is found for $\eta > \eta_c$, at first a complex sequence of chaotic and periodic motion, until eventually for large enough η the motion settles into a period-one motion that impacts precisely once per period. For $\hat{\theta} = 50°$ it was found that the pendulum amplitude is always less than the barrier angle $\theta(t) < \hat{\theta}$ for the forcing amplitude $A = 50.8$ mm, and hence no impacting motion takes place. We do not present results for this case.

Consider now the details of the four cases $\hat{\theta} = 10°$, 20°, 30°, 40° presented in panels (a)-(d) of Fig. 2. Note first that the frequency value of the grazing bifurcation η_c increases with $\hat{\theta}$.

At $\hat{\theta} = 10°$, $\eta_c \approx 0.343$, at which value there is a sudden jump to impacting chaotic behaviour. Time-series data extracted from the dynamics are shown in Fig. 3(a), where the high frequency effects were filtered out. From this figure we note the quality of the data due to the high precision (single-turn) rotational potentiometer interfaced with LabVIEW software. A phase space reconstruction of this dynamics, using Taken's method of delays (with a delay of one quarter of a cycle) is shown in Fig. 3(b). This shows the characteristic shape of a strange attractor. At higher η ($0.35 < \eta < 0.36$) a significant window of *period-two* periodic motion is observed, culminating in a reverse super-critical period-doubling bifurcation to period-one impacting motion.

For $\hat{\theta} = 20°$, η_c is approximately 0.405 and after a brief interval of apparently chaotic behaviour, there is a significant η-window ($0.406 < \eta < 0.42$) of *period-three* motion. There then follows a long interval of chaotic behaviour (with possible small periodic windows). This culminates in a window of period-two motion which itself dies in a sudden abrupt jump (possibly through a small interval of chaos) to period-one non-impacting motion.

For $\hat{\theta} = 30°$, where $\eta_c \approx 0.435$, a pattern appears to be emerging, because after a brief interval of chaos there is a significant window ($0.44 < \eta < 0.45$) of *period-four* impacting motion (whose period was confirmed by looking at the phase space reconstruction). This is again followed by a long interval of chaos, a period-two window and the eventual jump to the period-one non-impacting motion.

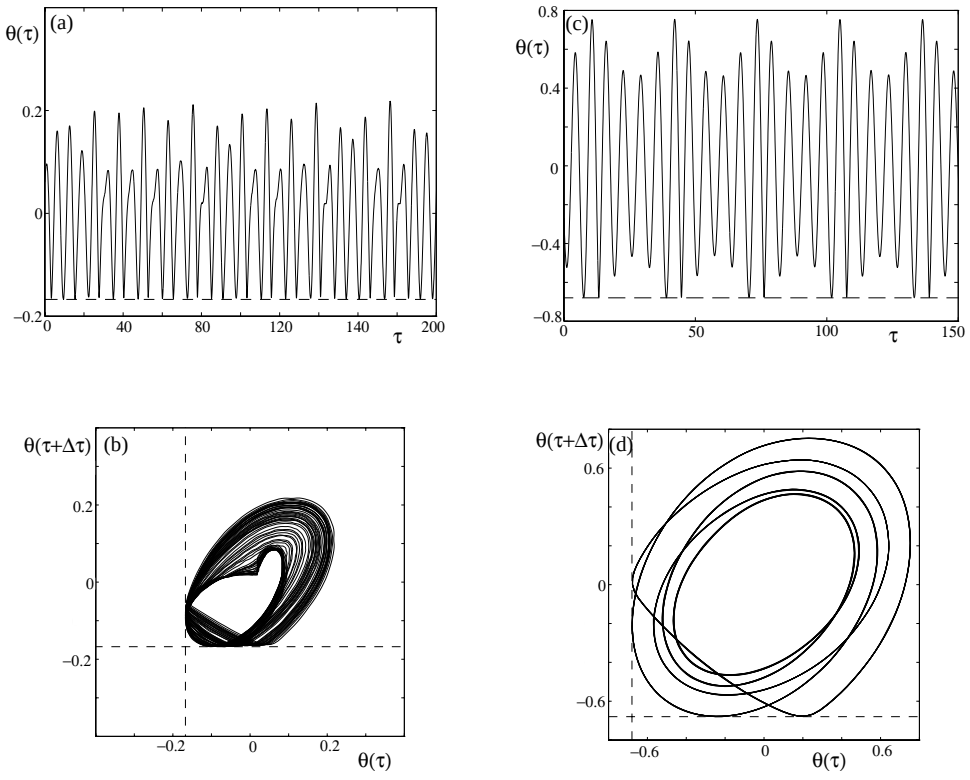

Figure 3: *Sample experimental time series and phase projections. (a) and (b)* $\hat{\theta} = 10°, \eta = 0.35$*; (c) and (d)* $\hat{\theta} = 40°, \eta = 0.45$.

The case $\hat{\theta} = 40°$, for which $\eta_c \approx 0.446$, completes the pattern. The first

significant periodic window (starting around $\eta = 0.45$) contains a *period-five* orbit, which is confirmed by the time series and phase space reconstruction shown in Fig. 3(c),(d). Again there is an interval of chaos, a period-two window and a jump to period-one non-impacting motion.

In summary then, the results definitely do not represent what one would expect from the theory of unimodal maps (e.g. [12]) that is replicated in most smooth dynamical systems undergoing period doubling. Here we see a sudden jump to chaos, and, as $\hat{\theta}$ is increased, rather than a period doubling cascade, we see a so-called period-adding cascade where the first significant periodic window jumps from period 2, to 3, to 4, to 5. Finally we note that the period-two window is the last to be seen and (for all cases other than $\hat{\theta} = 10°$) this ends abruptly rather than in a reverse supercritical period doubling.

3 Mathematical model

Equations of motion for a forced, inclined pendulum may be derived using elementary methods;

$$-\frac{\ddot{d}(t)}{L}\cos(\theta) = \ddot{\theta} + \frac{g_e}{L}\sin(\theta) + \kappa\dot{\theta}. \tag{2}$$

Here $d(t) = A\sin(\omega t)$ is the applied forcing, L is the effective length of the pendulum arm, and g_e the effective gravity (cf. section 2.1). Dissipation is included via a simple linear term $\kappa\dot{\theta}$, as is often assumed, in order to model the various causes of damping (other than the restitution at impact). Following [4, 48] we will nondimensionalize (2) by letting

$$\eta = \frac{\omega}{\omega_0}, \quad \text{where} \quad \omega_0 = 2\sqrt{\frac{g_e}{L}}, \quad \tau = \omega t, \quad \alpha = \frac{A}{L}, \quad \beta = \frac{\kappa}{2\omega_0}. \tag{3}$$

Here ω_0 is the frequency of small amplitude motion of the impacting oscillator (when $\hat{\theta} = 0$), which is twice the natural frequency of the non impacting system. The nondimensionalized equation can then be written as

$$\theta'' + \frac{2\beta}{\eta}\theta' + \frac{1}{4\eta^2}\sin(\theta) = \alpha\cos(\theta)\sin(\tau), \tag{4}$$

where $'$ represents $d/d\tau$. These are then the equations of motion that hold between impacts, i.e. for $\theta < \hat{\theta}$.

At impact $\theta = \hat{\theta}$ we assume a simple restitution law. Let τ_{im} be the time at which impact occurs, then we suppose that dimensionless angular velocity is instantaneously reset according to

$$\theta'(\tau_{\text{im}}^+) \leftarrow -r\theta'(\tau_{\text{im}}^-), \quad 0 \le r \le 1, \tag{5}$$

where r is the *coefficient of restitution*.

Equations (4) and (5) represent the mathematical model that we will use for the numerical results using the methods outlined in the next section. It contains five dimensionless parameters, α, β, η, r and $\hat{\theta}$. In the experimental data the amplitude was set at $\alpha = 0.2258$, which we shall henceforth assume (but see Sect. 6.2 below), and η and $\hat{\theta}$ were used as the main control parameters. That leaves β and r,

both of which contribute to the measured damping ratio $D = 0.07$. Further, a straightforward analysis shows that, in the absence of energy loss at impact

$$D = \frac{\kappa}{4\omega_0} = \beta. \tag{6}$$

Figure 4(a) shows the result of the numerical solution of (5), (4) in the freely decaying case ($\alpha = 0$) with $\hat{\theta} = 0$ and $r = 0.7148$ and $\beta = 0.0426$ ($\kappa = 1.1$). Now it

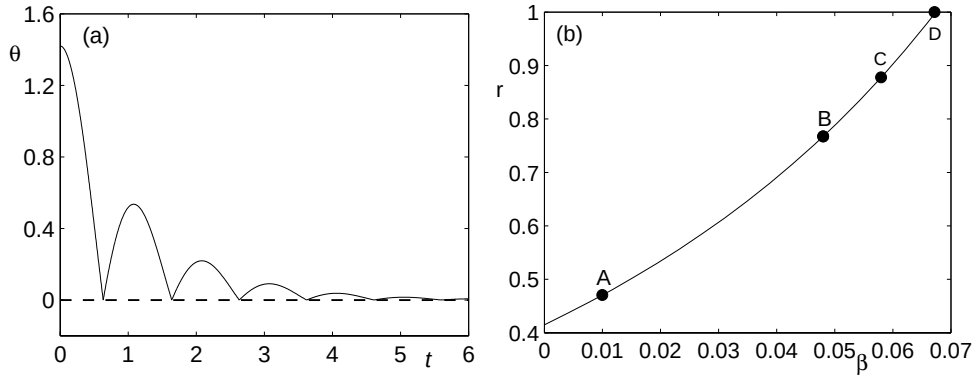

Figure 4: *(a) Free decay for an impacting pendulum with no forcing and where the coefficient of restitution* $r = 0.7148$ *and the damping coefficient* $\beta = 0.0426$*. (b) The relation between* r *and* β *to get a damping ratio that is* 7% *of critical. In (b) the letters 'A', 'B', 'C' and 'D' correspond to* $(r = 0.4707, \beta = 0.01)$*,* $(r = 0.7675, \beta = 0.048)$*,* $(r = 0.8778, \beta = 0.058)$*, and* $(r = 1, \beta = 0.68)$*, respectively.*

is possible to repeat this numerical experiment for different values of r and β and to measure the effective damping D according to the formula (1). In practice, the value of D was obtained by averaging over several peaks. In so doing, we are able to find a curve in the (r, β)-plane that corresponds to $D = 0.07$. The result is plotted in Fig. 4(b).

We see that when $\beta \approx 0.068$ then $r = 1$, which is unlikely in this experimental setup, and if no linear damping is assumed ($\beta = 0$) then the estimation of r is close to 0.42. A realistic choice of r for steel on steel contact lies somewhere between 0.5 and 0.8 (see for example [39, 33]), which corresponds to a linear damping coefficient β between 0.015 and 0.05. There would then appear to be a degree of freedom in choice of parameters in order to replicate the experimental set up. This was removed by a simple fitting procedure applied to the numerical replication of the experimental numerical results in Fig. 2(d) for $\hat{\theta} = 40°$, by ensuring that the primary grazing bifurcation happens for approximately the observed value of η (≈ 0.445). This results in the values of $r = 0.7675$ and $\beta = 0.048$ (corresponding to $\kappa \approx 1.238$), marked as point B on the curve in Fig. 4(b). Also marked are other values used for comparison in Sect. 6 below.

4 Numerical methods

We first discuss how to embed the impacting system within a numerical simulation framework, and then how to perform numerical path-following on the non-impacting orbits.

4.1 Simulation

Consider first the free motion between impacts (4). This can of course be rewritten as the system

$$x' = \begin{pmatrix} x_1' \\ x_2' \\ x_3' \end{pmatrix} = \begin{pmatrix} x_2 \\ \alpha\cos(x_1+\hat{\theta})\sin(x_3) - \frac{2\beta}{\eta}x_2 - \frac{1}{4\eta^2}\sin(x_1+\hat{\theta}) \\ 1 \end{pmatrix} := f(x), \quad (7)$$

where $x_1 = \theta - \hat{\theta}$, $x_2 = \theta'$, and $x_3 = \tau \mod 2\pi$. This definition of x_3 causes a jump in the state every time $x_3 = 2\pi$, but this discontinuity can be treated in the same way as the discontinuous jump, at impact, which we shall shortly discuss.

Since it is generally impossible to find explicit solutions to dynamical systems it is convenient to introduce the flow function Φ such that $\Phi(x_0, t-t_0)$ corresponds to the point at time t on the trajectory that passes through x_0 at time t_0. Let Φ_t denote $\frac{\partial}{\partial t}\Phi$, then in terms of the flow function a general dynamical system (including (7)) can be written as

$$\Phi_t(x, t-t_0) = f(\Phi(x, t-t_0)), \quad \Phi(x,0) = x_0 \quad (8)$$

for all x and t, and the unique solution to (7) is given by $x(t) = \Phi(x_0, t-t_0)$.

In order to implement impact detection we introduce the function

$$h_{\text{im}}(\theta(t)) = \theta - \hat{\theta} \equiv h(x) = x_1.$$

In practice, then time, angle, and angular velocity of the pendulum at impact is found by monitoring $h_{\text{im}}(x(t))$ during the integration of (7), and when $h_{\text{im}} = 0$ the impact law (5) is applied. Thus effective simulation of the combined hybrid system can occur. In the results that follow this is implemented in MATLAB using `ode45` with accurate hit-crossing to detect zeros of h_{im}.

4.2 Continuation and stability of periodic orbits

In order to apply the normal form theory that follows we need to accurately detect periodic solutions, perform continuation of them up to a grazing bifurcation, at which point we also need the linearisation around the periodic orbit. In fact, we derive a more general method for continuation of periodic solutions to hybrid systems of the form

$$\dot{x} = f(x), \quad h(x) > 0, \quad (9)$$

where $x \in \mathbb{R}^n$ is the state, subject to the impact law

$$x(t_{\text{im}}^+) \leftarrow g(x(t_{\text{im}}^-)), \quad h(x) = 0. \quad (10)$$

By definition, for a periodic orbit, it is possible to find at least one x^* on the orbit such that

$$x^* = \Phi(x^*, T), \quad (11)$$

where $T > 0$ is the period (cf. Fig. 5 (a)). Consider a periodic orbit that impacts just once per period. Then, from (11) there exists a time t_{im}, such that $h(\Phi(x^*, t_{\text{im}})) = 0$ and

$$x^* = \Phi_2(g(\Phi_1(x^*, t_{\text{im}})), T - t_{\text{im}}), \quad (12)$$

where Φ_1 and Φ_2 are the flow functions before and after the interaction with $h = 0$, respectively (cf. Fig. 5 (c)). Similar defining equations hold for $m > 1$ impacts, but with $m + 1$ flow functions $\Phi_1, \ldots, \Phi_{m+1}$, m jump functions $g_1, \ldots, g_m$, and m times $t_{\mathrm{im},1}, \ldots, t_{\mathrm{im},m}$. However, here we shall focus on periodic orbits with at most one impact per period and for which only one flow rule applies, so that $\Phi_1 = \Phi_2 = \Phi$.

Below we let $\Psi(x^*, T)$ denote either the right hand side of (11) or (12), i.e. it could be either a smooth or piecewise smooth function.

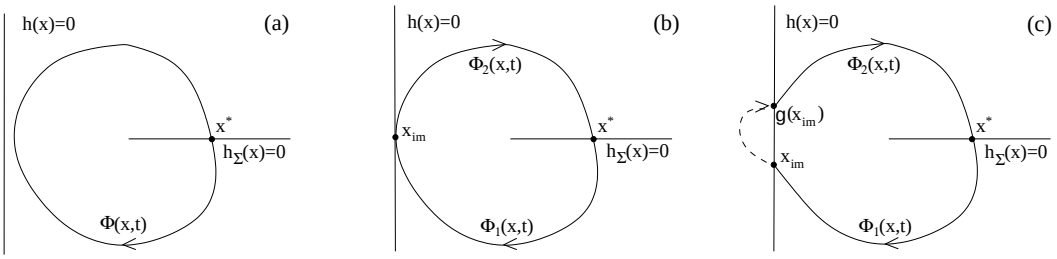

Figure 5: *Periodic orbits with (a) no impacts, (b) grazing, and (c) impact once a period.*

To locate periodic motions with or without discontinuous jumps in the states, i.e. to solve eqs. (11) or (12), we will use Newton's method. This method requires the calculation of the Jacobian $\Psi_x(x^*, T)$, the derivative of the flow Ψ with respect to the state x over one period including discontinuous jumps. Following [23, 44, 10], the Jacobian for a periodic orbit with a single impact is

$$\Psi_x(x^*, T) = \Phi_{2,x}(g(x_{\mathrm{im}}), T - t_{\mathrm{im}}) G(x_{\mathrm{im}}) \Phi_{1,x}(x^*, t_{\mathrm{im}}), \tag{13}$$

where the two Jacobians $\Phi_{1,x}$ and $\Phi_{2,x}$ are solutions to the first variational equations before and after the impact and

$$G(x_{\mathrm{im}}) = g_x(x_{\mathrm{im}}) + \frac{f(g(x_{\mathrm{im}})) - g_x(x_{\mathrm{im}}) f(x_{\mathrm{im}})}{h_x(x_{\mathrm{im}}) f(x_{\mathrm{im}})} h_x(x_{\mathrm{im}}), \tag{14}$$

where h_x and g_x are derivatives of the functions h and g with respect to the state x, respectively, and where

$$h_x(x_{\mathrm{im}}) f(x_{\mathrm{im}}) \neq 0.$$

The function $G(x_{\mathrm{im}})$ can be derived by using a zero-time discontinuity mapping approach (see [19, 10] and Sect. 5) and takes into account both changes in the state and vector field before and after the discontinuous jump. This matrix is sometimes referred to as the saltation matrix [31]. Also, since both equations (11) (non-impacting) and (12) (impacting) consist of n equations for the unknowns we need to add an extra equation to find a unique periodic solution. A natural choice is a function $h_\Sigma(x) = 0$ that defines a Poincaré surface Σ. Thus, the equations we want to be fulfilled for a periodic orbit are

$$\Psi(x^*, T) = x^*, \tag{15}$$

and

$$h_\Sigma(x^*) = 0. \tag{16}$$

By using eqs. (13-16) Newton's method can be formulated as

$$\begin{pmatrix} x_{k+1} \\ T_{k+1} \end{pmatrix} = \begin{pmatrix} x_k \\ T_k \end{pmatrix} - \begin{pmatrix} \Psi_x(x_k, T_k) - I & \Psi_t(x_k, T_k) \\ h_{\Sigma,x}(x_k) & 0 \end{pmatrix}^{-1} \begin{pmatrix} \Psi(x_k, T_k) - x_k \\ h_\Sigma(x_k) \end{pmatrix}, \tag{17}$$

where $\Psi_t(x_k, T_k) = f(x_k)$ is the vector field on the surface Σ at the point x_k. When both $\|x_{k+1} - x_k\|$ and $\|T_{k+1} - T_k\|$ are sufficiently small (within a given tolerance) we choose to let $x^* = x_{k+1}$ be the periodic point on the surface Σ and $T = T_{k+1}$ its period. Whenever a periodic orbit has been located the linear stability of this orbit is given by the Floquet multipliers (i.e. the eigenvalues of the flow Jacobian $\Psi_x(x^*, T)$).

For the parameter continuation of periodic orbits any path-following method can be used. Specifically we have implemented the pseudo-arclength method (see [27, 29]). The resulting code has been written in MATLAB and can be used to additionally follow an additional constraint in two parameters, such as the condition that grazing occurs at t_{im}.

5 The grazing bifurcation normal form

To study grazing motions it is convenient to introduce a local transversal Poincaré surface (as in the previous section) through a point on the grazing trajectory that is not on the impacting surface, such that a periodic motion with grazing impacts becomes a fixed point of the Poincaré mapping (cf. Fig. 5(b)). Motions with grazing impacts are sensitive to small perturbations, i.e. trajectories starting in a vicinity of the gracing trajectory can experience a low-velocity impact, grazing impact, or no impact at all. Despite this, low-velocity impacts lead to continuous, but non-differentiable, Poincaré maps. Therefore, following Nordmark [34, 19] the low-velocity impacts can be treated separately from the rest of the motion by introducing, so called, *discontinuity maps*.

We first summarize what is known for general hybrid dynamical systems of the form (11) subject to an impact law of the form (10). In fact we shall make a minor restriction on the form of restitution function g

$$x \leftarrow g(x) = x + e(x)\mathcal{L}_f h(x), \tag{18}$$

where

$$\mathcal{L}_f h(x) = h_x x' = h_x f(x)$$

is the Lie derivative of h, the function defining the impacting surface, with respect to the vector field and gives the direction in which the impact law is applied, e is the amount the state is changed and will here depend on the coefficient of restitution r, and h_x is the derivative of h with respect to x. We assume that $x_{\rm im}$ is the point of grazing, i.e. $h(x_{\rm im}) = 0$. Under these assumptions, the method in ref. [35, 36] allows one to write down the local discontinuity mapping for low-velocity impacts as

$$D(x) = \begin{cases} x + b(x, y)y, & h(x) \le 0, \\ x, & h(x) > 0, \end{cases} \tag{19}$$

where

$$y = \sqrt{-h(x)} \quad \text{and} \quad b(x_{\rm im}, 0) = -\sqrt{2\mathcal{L}_f^2 h(x) e(x)|_{x=x_{\rm im}}}.$$

One way to interpret this mapping is that, by using the flow functions, the complete Poincaré map around the periodic orbit can be written as

$$\Pi(x,T) = \Phi_2(D(\Phi_1(x,t_{\rm im})), T - t_{\rm im}), \tag{20}$$

where $T > 0$ is the period of the grazing periodic orbit and $t_{\rm im}$ is the time ($0 < t_{\rm im} < T$) when the grazing impact occurs.

In order to apply this discontinuity map to the impacting pendulum system (4) and (5), we must first write the impact law in the form (18). Specifically, at impact we have

$$\begin{pmatrix} x_1 \\ x_2 \\ x_3 \end{pmatrix} \leftarrow \begin{pmatrix} x_1 \\ -rx_2 \\ x_3 \end{pmatrix}. \tag{21}$$

Hence, since we have

$$h_x = (1,0,0), \quad \mathcal{L}_f h(x) = h_x f(x) = x_2, \quad e(x) = (0,-(1+r),0)^T,$$

we have that

$$b(x_{\rm im},0) = -\sqrt{2\mathcal{L}_f^2 h(x)} e(x)|_{x=x_{\rm im}} = -\sqrt{2a(x_{\rm im})}(0,-(1+r),0)^T, \tag{22}$$

where $a = x_2'$ given by the second component of the right-hand side of (7) and $x_{\rm im} = (0,0,t_{\rm im})^T$ Finally, from eqs. (18 - 20), and (22) the Poincaré map for the full orbit is given by

$$\Pi(x,T) = \Phi_2(D(\Phi_1(x,t_{\rm im})), T - t_{\rm im}), \tag{23}$$

where

$$D(x) = \begin{cases} x + \begin{pmatrix} 0 \\ 1+r \\ 0 \end{pmatrix} \sqrt{-2x_1 a(x_{\rm im})}, & h(x) \le 0, \\ x, & h(x) > 0, \end{cases} \tag{24}$$

and where we have used $y = \sqrt{-x_1}$.

We are now in a position to use this map to estimate the behavior of motions near grazing. The estimations will be compared with experimental results and direct numerical simulations.

6 Results

In this section we will compare direct numerical simulations with the experimental results shown in Sect. 2 and the mapping derived in the previous section. Grazing periodic orbits will be continued and the ability to calculate the stability will be used to explain the period adding cascade shown in the bifurcation diagrams. Further we will discuss parameter dependence and how small parameter variations influence the dynamics in resonant regions.

6.1 Numerical results

Let us first take a look at non-impacting motion which is the key to revealing what happens in systems including low-velocity impacts. Figure 6 shows variation in the maximum amplitude of the stable period-one non-impacting motion for the four

different values of the damping parameter illustrated in Fig. 4(b). Note that these response curves are obtainable analytically and show a characteristic fundamental resonance peak close to $\eta = 0.5$. For now, let us focus on case B ($\beta = 0.048$) which we obtained by parameter fitting the η-value of the first grazing bifurcation for the case $\eta = 0.4$. The values of the varying impact stop angle $\hat{\theta}$ are depicted as horizontal lines in the figure at 10° intervals. Hence the η-values at which the first and second grazing bifurcations (which respectively destroy and create period-one nonimpacting motion) can be read off from the graph as in intersection between the response curve and the appropriate horizontal line. The right panel of Fig. 6 shows the same response curve computed by numerical continuation, in which we have also computed the Floquet multipliers of the periodic orbit which are depicted at three points along the curve.

The first thing to note from Fig. 6 is that there is an upper bound of $\hat{\theta}_{\max}$ beyond which grazing cannot occur for any value of η (about 55° for case B). Another thing to note is that for $\hat{\theta} = 10°$ there is no second grazing bifurcation to restore period-one nonimpacting motion. Both of these accord with what was observed the experimental data (although the upper bound of 55° is somewhat higher than that observed experimentally).

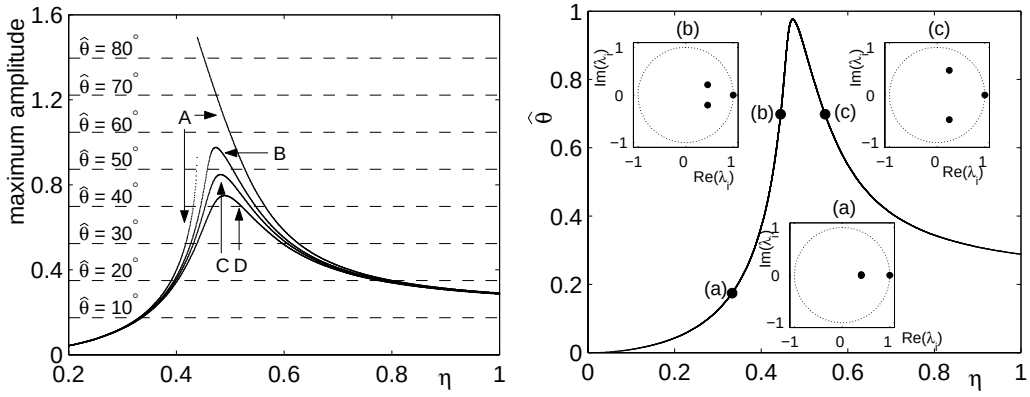

Figure 6: *Left: Long time behaviour of the non-impacting pendulum for four different damping parameters β. The letters A, B, C, and D correspond to $\beta = 0.010$, $\beta = 0.048$, $\beta = 0.058$, and $\beta = 0.068$, respectively. Right: Two-parameter (in η and $\hat{\theta}$) continuation of grazing periodic orbits where $r = 0.7675$ and $\beta = 0.048$. The corresponding Floquet multipliers λ_i are shown in the insets for (a) $\hat{\theta} = 10°, \eta = 0.3229$, (b) $\hat{\theta} = 40°, \eta = 0.4450$, and (c) $\hat{\theta} = 40°, \eta = 0.5475$. The values of the Floquet multipliers are (a) $(1, 0.4040 \pm 0.0114i)$, (b) $(1, 0.4606 \pm 0.2137i)$, and (c) $(1, 0.2534 \pm 0.5178i)$.*

Next we present the results of numerical simulation of the equations (4), (5), sticking to case B of the damping and restitution coefficients. Figure 7 shows Poincaré section brute-force bifurcation diagrams over the same frequency range and values of $\hat{\theta}$ as in the experimental data.

We see the same broad features of the dynamics upon increasing η as was observed in the experiment. For each $\hat{\theta}$ there is a first grazing bifurcation that leads to a rapid change in the dynamics, from non-impacting period-one periodic motion to impacting chaotic motion containing windows of stable periodic orbits in a

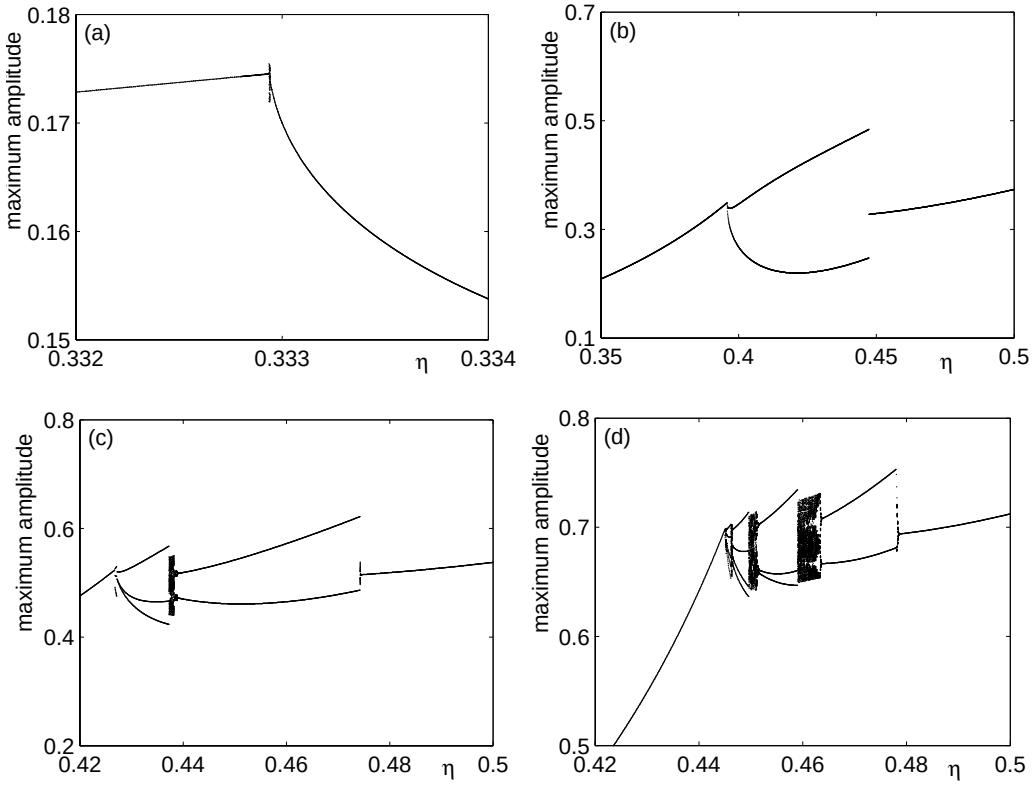

Figure 7: *Changes in existence and stability of the forced impacting pendulum under variation of η and where (a) $\hat{\theta} = 10°$, (b) $\hat{\theta} = 20°$, (c) $\hat{\theta} = 30°$, and (d) $\hat{\theta} = 40°$ using direct numerical simulation. The coefficient of restitution $r = 0.7675$, the damping coefficient $\beta = 0.048$, and the forcing amplitude $\alpha = 0.2254$.*

period-adding cascade. The period is decreased by one for each periodic window as η is increased (a reverse period doubling cascade). As in the experimental results, the period of the first appreciable periodic window is increasing with increasing $\hat{\theta}$, for a specific η; in this case period-one for 10°, two for 20°, three for 30° and four (actually, briefly, five) for 40°

The period-adding cascade is clearly highlighted in Fig. 8(a), which was calculated similarly to Fig. 7, but here η is held fixed at 0.447 while $\hat{\theta}$ is varied. We now observe a grazing bifurcation at $\hat{\theta} = 41°$ as the onset of a period adding cascade, where the period increases with $\hat{\theta}$.

Returning to Fig. 7, notice for all cases with $\hat{\theta} > 10°$ the region of impacting behaviour ends with another grazing bifurcation which results in the destruction of a period-two orbit, just as in the experimental data.

In Figs. 9(a) and 9(b) numerical time series are shown for two different cases, $(\hat{\theta} = 10°, \eta = 0.33294)$ and $(\hat{\theta} = 40°, \eta = 0.446)$, respectively, which qualitatively correspond to the experimental time series shown in Fig. 3(a) and 3(c). On one hand, the numerical and experimental results have similar amplitude, but on the other hand there are some differences in the dynamical characteristics between the numerical and experimental results. These differences have their origins in the differences in the bifurcation diagrams at the particular η-values given above. As an

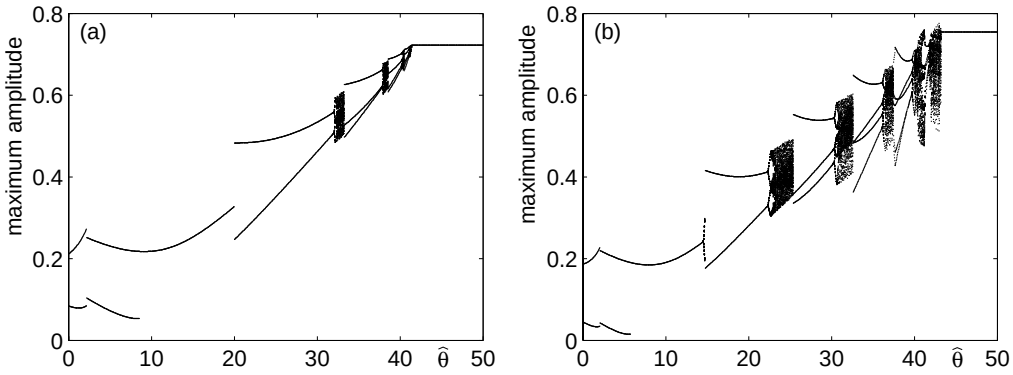

Figure 8: *Bifurcation diagrams of the forced impacting pendulum under impact barrier angle $\hat{\theta}$ variation where $\eta = 0.447$. In (a) $r = 0.7675$, $\beta = 0.048$ and in (b) $r = 0.4707$, $\beta = 0.01$. The figures (a) and (b) correspond to case B and case A in the right panel of Fig. 6, respectively.*

example, in Fig. 3(d) the experiment shows a period-five motion but the numerics a chaotic motion for the same η-value, which can be seen in the corresponding bifurcation diagram in Fig. 7(d). However, if η is slightly changed (from 0.45 to 0.446) the numerical simulation gives the same motion characteristics (period-five motion) as the experiment.

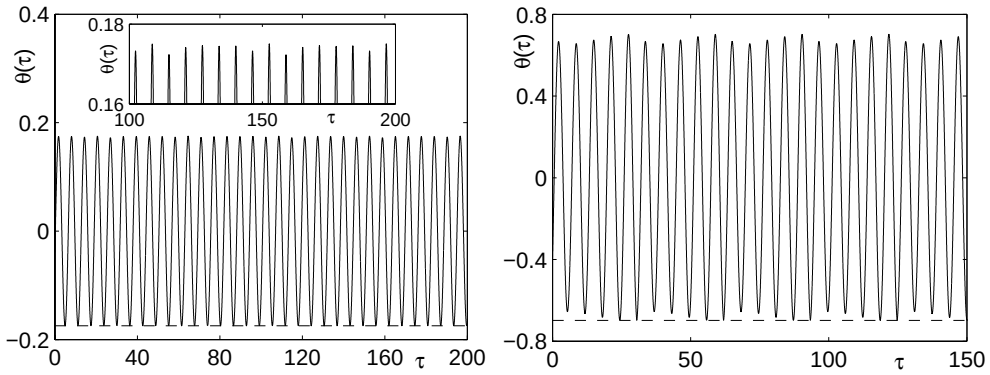

Figure 9: *Sample numerical time series corresponding to the experimental shown in Fig. 3, where (a) $\hat{\theta} = 10°$, $\eta = 0.33294$, and (b) $\hat{\theta} = 40°$, $\eta = 0.446$. In (a) the motion is chaotic and in (b) period-5. The inset in (a) is a magnification of the upper part of the time series and visualizes the chaotic motion.*

Next we will examine how well the Poincaré map Π, given by (23), derived in Sect. 5 predicts the dynamics caused by the first grazing bifurcation. The main ingredient required to compute this map is the computation of the linearisation around the grazing periodic orbit. This can be obtained for free from the Jacobian matrix if the periodic orbit is continued using the methods discussed in Sect. 4.2. The results of a two-parameter continuation (in $\hat{\theta}$ and η), of the grazing period-one orbit were already shown in the right panel of Fig. 6, together with the corresponding Floquet multipliers. We note that one multiplier is always identical to unity, as it

should be, and the other two lie within the unit circle indicating that the orbits are stable. For most parameter values of interest, these two nontrivial multipliers are complex.

Let us focus on the first grazing bifurcation for $\hat{\theta} = 40°$, at $\eta = 0.445$, for which the magnitude of the (largest in magnitude) non-trivial multiplier is $|\lambda| = 0.5114$ (see inset (b) of Fig. 6). Now, grazing bifurcation theory [8, 18, 37] predicts that if

$$\frac{1}{4} < |\lambda| < \frac{2}{3} \tag{25}$$

then the bifurcation will cause the onset onset of a period adding cascade, which is exactly what we see in Fig. 7(d).

Figures 10(a)-(d) uses the local discontinuity mapping approach to recreate the bifurcation diagrams in Fig. 7. Even though the discontinuity mapping approach is local, the qualitative agreement between the two different methods is good even for η-values relatively far away from the point of grazing. For instance, the period adding cascades are captured and clearly visible in Fig. 10(c) and (d), but the intervals in which they appear are somewhat shortened.

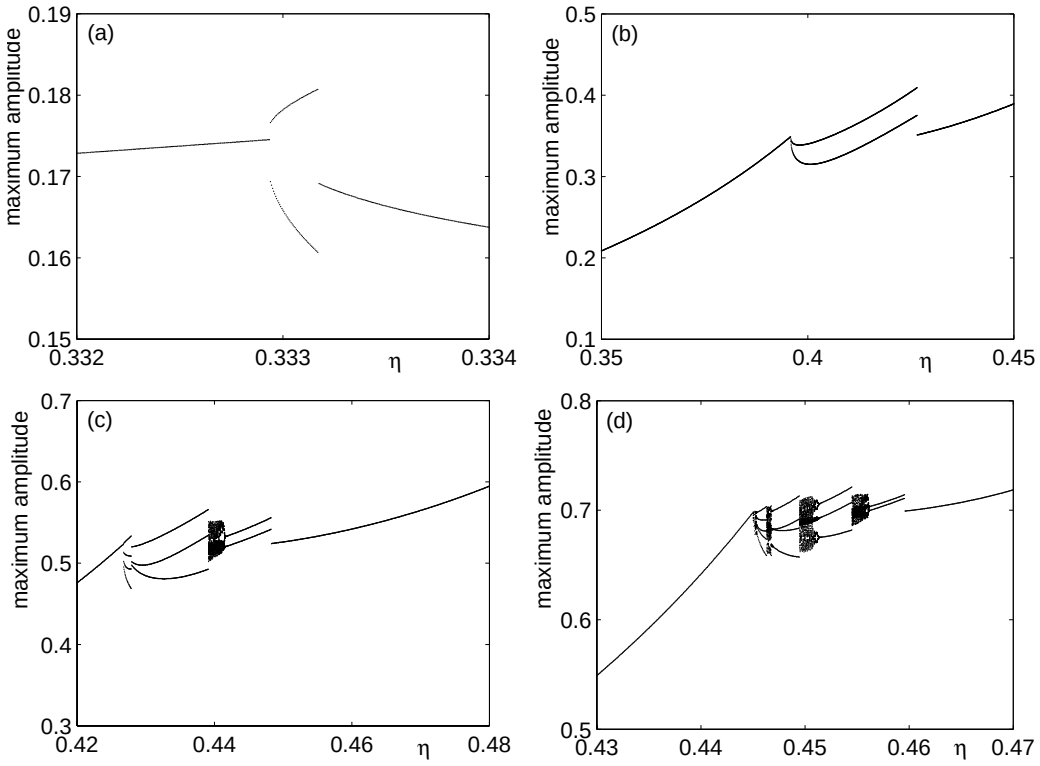

Figure 10: *The same results as in Fig. 7 but computed using the discontinuity mapping*

To further highlight how grazing and low-velocity impact influence the overall dynamics, we can use the map Π to compute the shape of the chaotic attractor. Fig. 11(b) shows a delay plot (two consecutive iterates of the map; θ_{k+1} against θ_k) for $\hat{\theta} = 40°$ and $\eta = 0.4458$, i.e. just beyond the first grazing bifurcation). Fig. 11(a) shows the same information computed by direct numerical simulation of the equations (4) and (5) using the Poincaré section $\{x_3 := \tau = 0\}$. The agreement

between the two is plain to see. For both, the characteristic fingered appearance of the attractor is clearly visible. The almost vertical branches on the left hand side causes the stretching in the state space (and the chaotic dynamics) and can be explained by the square root term in the local map for grazing impacts, as discussed in Sect. 5. The reason for the appearance of a number of parallel branches in the delay plot indicates that the global Poincaré map Ψ is not one-dimensional, which we know to be true.

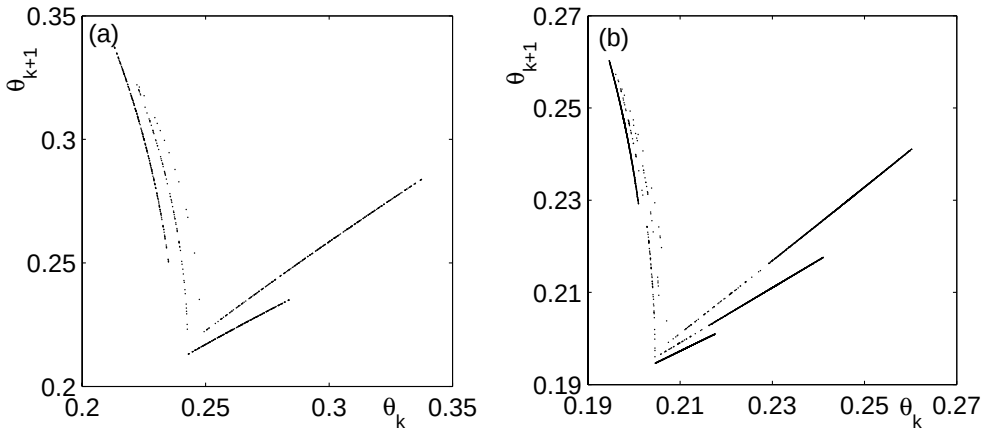

Figure 11: *Delay plots for the impacting pendulum near grazing using (a) direct numerical simulation and (b) discontinuity map at Poincaré section* $h(x) = x_3 = 0$. *In both cases* $r = 0.7675$, $\beta = 0.048$, $\eta = 0.4458$.

Finally consider the reverse grazing bifurcation that occurs for $\eta = 0.5475$ when $\hat{\theta} = 40°$. Here the magnitude of the non-trivial Floquet multipliers satisfies $|\lambda| = 0.5765$ (see inset (c) of Fig. 6). Note that, compared with the first grazing bifurcation, this is closer to the upper threshold in (25) for the existence of period-adding cascades according to the theory of grazing bifurcations. This goes some way to explain why the transition back to non-impacting behaviour is much more sudden and does not appear to involve any appreciable chaotic behaviour.

6.2 Parameter uncertainty

Looking at Fig. 6 we note just how sensitive the height of the resonance peak is to the value of the damping parameter. This has strong implications for the location of the first grazing bifurcation, and indeed for the value $\hat{\theta}_{\max}$ beyond which grazing cannot occur. This also implies that the linearisation around the grazing periodic orbits is highly sensitive to damping, which can cause gross changes in the details of the period-adding cascade close to the grazing point.

To test this sensitivity we have varied the parameters β and r along the curve in Fig. 4(b) and found no significant difference in the qualitative picture of the bifurcation diagrams, but large quantitative differences. Figures 8(a) and (b) compare bifurcation diagrams, where the impact barrier angles are varied for fixed $\eta = 0.447$, in damping cases B and A from Fig. 4(b), respectively. Both show period adding cascades, but the case with smaller β has significantly wider intervals of chaos and also wider, more appreciable windows of the higher-period periodic windows. These latter results would appear to echo what is observed in the experimental data. Nev-

ertheless, we have not been able to find a single point on the (r, β) curve that gives a perfect fit between the numerical and experimental results. In particular, although there is better agreement with the experimental data using case A than case B, this greatly overestimates the value of $\hat{\theta}_{\max}$ observed experimentally (recall that no impacting behaviour was observed for $\hat{\theta} = 50°$). There might be a number of reasons for this other than uncertainty in the damping and restitution parameters, such as vibrations in the experimental setup, errors in the parameter measurements, or wrong assumptions in the mathematical modeling (for example damping may enter through a nonlinear velocity-dependent term due to coulomb friction in the pivot).

To highlight this uncertainty, we have performed numerical experiments with a lower value of forcing amplitude 0.71α, keeping the coefficient of restitution $r = 0.4707$ and the damping coefficient $\beta = 0.01$ fixed (case A). One can argue that this is effectively similar to increasing the overall damping in the structure, since both have the effect of lowering the amplitude of the resonance peak. The resulting bifurcation diagrams under η variation for $\hat{\theta} = 10°, 20°, 30°, 40°$ are shown in Figs. 12(a)-(d), respectively. If we now compare these results with the experimental bifurcation diagrams in Figs. 2(a)-(d) the match is a lot better than what was seen in Figs. 7(a)-(d). With this perturbed amplitude and with $\hat{\theta} = 10°$(a), $40°$(d) the bifurcation diagrams are uncannily similar to those observed in the experiments, and even in the other two cases we can clearly see one large periodic window surrounded by chaotic regions, culminating in a period-two window.

7 Discussion

This paper has sought to use the experimental data from a careful experiment on a one degree-of-freedom impacting pendulum in order to justify the approach that has become standard in the study of grazing bifurcations, namely to derive the square-root normal-form map using Nordmark's idea of the discontinuity mapping. These days, one has come to expect chaotic dynamics in forced pendulum systems, but perhaps the most striking feature of the experimental results are the sudden abrupt jump to chaos and the cascade of period windows whose period increase by one cycle in subsequent windows (a so-called period adding cascade). This is precisely the dynamics that the grazing bifurcation normal form predicts. Moreover we have attempted a quantitative explanation of the experimental observations, via direct numerical simulations, periodic orbit continuations methods, and careful construction of the discontinuity mappings. One side result has been to show just how good a match can be found between the discontinuity mapping approach and the direct numerical simulation. In seeking a match with the experimental data, we have indeed found that the normal form is precisely in the right region for period-adding and chaos to occur, but a precise quantitative fit is more troublesome (these conclusions echo those in a similar study [20], in which impacts of a pipe conveying fluid are analyzed experimentally and numerically)

Our results have highlighted the crucial role played by damping in organizing the finer features of the observed dynamics. Of course, the coefficient of restitution associated with impact causes damping of the impacting behaviour. So, in previous studies that have considered experimental comparison with dynamics that always impacts (e.g. [39]) it was not so crucial whether damping is taken account of via restitution or a linear viscous term. However, in this study we have been interested in precisely the transition between non-impacting and impacting behaviour and so

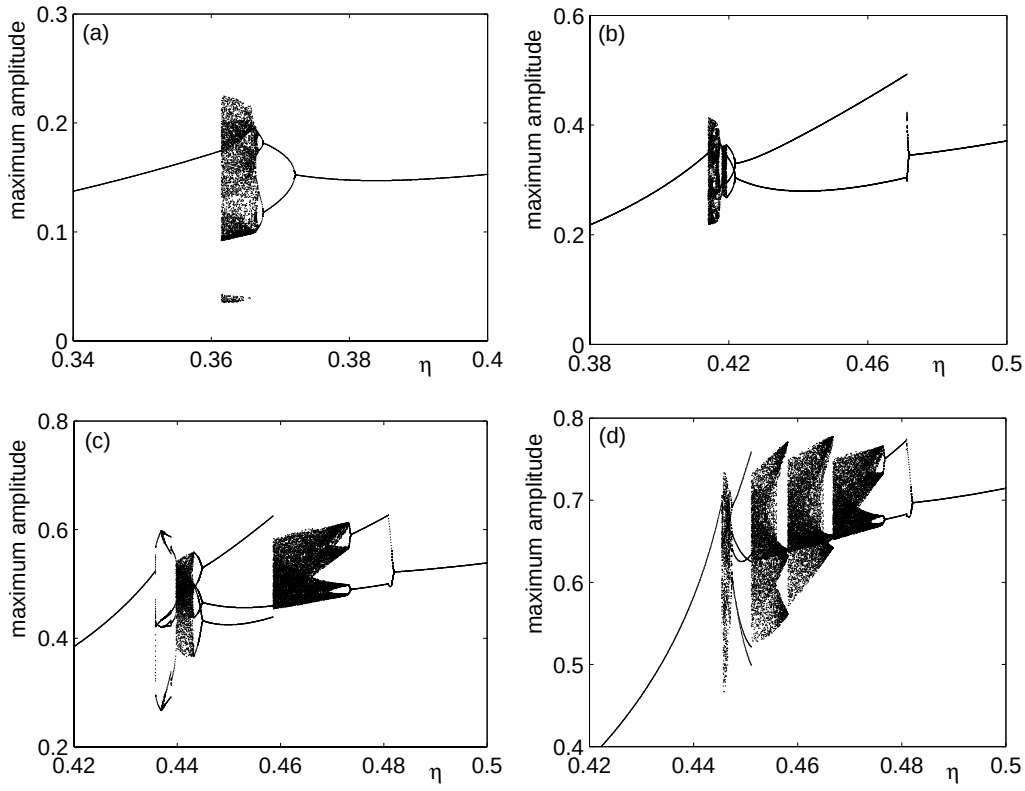

Figure 12: *Changes in existence and stability of the forced impacting pendulum under variation of* η *and where* $\hat{\theta} = 10^\circ$ *(a),* $\hat{\theta} = 20^\circ$ *(b),* $\hat{\theta} = 30^\circ$ *(c), and* $\hat{\theta} = 40^\circ$ *(d). The driving frequency is* 0.71α*, the coefficient of restitution* $r = 0.4707$ *and the damping coefficient* $\beta = 0.01$*.*

both viscous and restitution damping play a crucial role. However, as the final results produced in the previous section show (see Fig. 12), the key to obtaining close quantitative agreement with the experiments is to get the correct amplitude of the pre-impacting orbit, which in this case was obtained by adjusting the forcing amplitude from its true value. As already intimated, this effective amplitude adjustment may be due to the damping occurring via effects that we have not modelled such as nonlinear coulomb friction, or structural interactions.

This paper also shows the importance of careful parameter value estimations, when trying to explain experimental results using a mathematical model, especially ones that exhibit the infinite local stretching inherent in the square-root map. Often one can use simplified models with an essential few parameters, but it is also likely that the original real-world system has a large number of significant parameters that cannot easily be simplified or ignored. Even worse, some of the parameters can have a stochastic behavior (due to noise from various sources) which require analysis using methods that goes beyond this paper.

Acknowledgment

This work was supported by the EU FP5 Project SICONOS (Grant no. IST-2001-37172). Arne Nordmark is acknowledged for sharing his insights into grazing bifurcations.

References

[1] M. A. Aizerman and E. S. Pyatnitskii. Foundations of a theory of discontinuous systems. I–II. *Automation and Remote Control*, 35(7):1066–1079, 1242–1262, 1974.

[2] V. I. Babitskii. *Theory of Vibroimpact Systems. Approximate methods*. Nauka, Moscow, 1978.

[3] Halliwell NA Batako AD, Babitsky VI. A self-excited system for percussive-rotary drilling. *J. Sound Vib.*, 259, 2003.

[4] P V Bayly and L N Virgin. An experimental study of an impacting pendulum. *Journal of Sound and Vibration*, 164(2):364–374, 1993.

[5] B. Brogliato. *Nonsmooth Mechanics – Models, Dynamics and Control*. Springer–Verlag, New York, 1999.

[6] C. J. Budd and F. Dux. Chattering and related behaviour in impact oscillators. *Phil. Trans. Roy. Soc. Lond. A*, 347:365–389, 1994.

[7] D.R.J. Chillingworth. Discontinuity geometry for an impact oscillator. *Dynamical Systems*, 17:380–420, 2002.

[8] W. Chin, E. Ott, H. E. Nusse, and C. Grebogi. Grazing bifurcations in impact oscillators. *Physical Review E*, 50:4427–4444, 1994.

[9] H. Dankowicz and A. B. Nordmark. On the origin and bifurcations of stick-slip oscillations. *Physica D*, 136:280–302, 1999.

[10] H. Dankowicz and P.T. Piiroinen. Exploiting discontinuities for stabilization of recurrent motions. *Dynamical Systems*, 17:317–342, 2002.

[11] J. H. B. Deane and D. C. Hamill. Analysis, simulation and experimental study of chaos in the buck concerter. In *Proceedings of the Power Electronics Specialists Conf. (PESC 1990)*, pages 491–8, New York, 1990. IEEE Press.

[12] R.L. Devaney. *An introduction to chaotic dynamical systems*. Addison-Wesley, Reading, Mass., second edition, 1989.

[13] M. di Bernardo, C. J. Budd, and A. R. Champneys. Corner–collision implies border–collision bifurcation. *Physica D*, 154:175–194, 2001.

[14] M. di Bernardo, M. I. Feigin, S. J. Hogan, and M. E. Homer. Local analysis of C-bifurcations in n-dimensional piecewise smooth dynamical systems. *Chaos, Solitons and Fractals*, 10:1881–1908, 1999.

[15] M. di Bernardo, P. Kowalczyk, and A. Nordmark. Bifurcations of dynamical systems with sliding: derivation of normal-form mappings. *Physica D*, 170:175–205, 2002.

[16] M. I. Feigin. Doubling of the oscillation period with C-bifurcations in piecewise continuous systems. *PMM*, 34:861–869, 1970. In Russian.

[17] M. I. Feigin. *Forced Oscillations in Systems With Discontinuous Nonlinearities*. Nauka, Moscow, 1994. In Russian.

[18] M. H. Frederiksson and A. B. Nordmark. Bifuractions caused by grazing incidence in many degrees of freedom impact oscillators. *Proc. Royal Soc. Lond. A*, 453:1261–1276, 1997.

[19] M. H. Frederiksson and A. B. Nordmark. On normal form calculations in impact oscillators. *Proc. Royal Soc. Lond. A*, 456:315–329, 2000.

[20] M H Fredriksson, D Borglund, and A B Nordmark. Experiments on the onset of impacting motion using a pipe conveying fluid. *Nonlinear Dynamics*, 19:261–271, 1999.

[21] H. Goyder and C. Teh. A study of the impact dynamics of loosely supported heat exchanger tubes. *J. Pressure Vessel Technology*, 111:394–401, 1989.

[22] J. Guckenheimer and P. Holmes. *Nonlinear Oscillations, Dynamical Systems, and Bifurcations of Vector Fields*. Springer–Verlag, New York, 1983. Applied Mathematical Sciences, Volume 42.

[23] Adolfsson J., Dankowicz H., and Nordmark A. 3D passive walkers: Finding periodic gaits in the presence of discontinuities. *Nonlinear Dynamics*, 24:205–229, 2001.

[24] J. Jerrelind and A. Stensson. Braille printer dynamics. In *Proceedings of 1999 ASME Design Engineering Technical Conferences*, 1999.

[25] J. Jerrelind and A. Stensson. Nonlinear dynamic behaviour of coupled suspension systems. *Meccanica*, 38:43–59, 2003.

[26] A. Kaharaman and R. Singh. Nonlinear dynamics of a spur gear pair. *J. Sound Vib.*, 142:49–75, 1990.

[27] H B Keller. *Lectures on Numerical Methods In Bifurcation Problems*. Springer-Verlag, 1987.

[28] A.M. Krivtsov and M. Wiercigroch. Dry friction model of percussive drilling. *Meccanica*, 34, 1999.

[29] Yu A. Kuznetsov. *Elements of Applied Bifurcation Theory*. Springer–Verlag, New York, second edition, 1998. Applied Mathematical Sciences, Volume 112.

[30] Yu.A. Kuznetsov, S. Rinaldi, and A. Gragnani. One-parameter bifurcations in planar fillipov systems, 2003. To appear in *Int. J. Bifurcation Chaos*.

[31] R Leine. *Bifurcations in Discontinuous Mechanical Systems of Filippov-Type*. PhD thesis, Teknische Universiteit Eindhoven, The Netherlands, 2000.

[32] T. McGeer. Passive dynamic walking. *Int. Journal of Robotics Research*, 9:62–82, 1990.

[33] J. L. Meriam and L. G. Kraige. *Engineering Mechanics: Dynamics*, volume 2. Wiley, fifth edition, 2003.

[34] A. Nordmark. *Grazing conditions and chaos in impacting systems.* PhD thesis, Royal Institute of Technology, Stockholm, Sweden, 1992.

[35] A. B. Nordmark. Non-periodic motion caused by grazing incedence in an impact oscillator. *Journal of Sound and Vibration*, 145(2):279–297, 1991.

[36] A. B. Nordmark. Universal limit mapping in grazing bifurcations. *Physical Review E*, 55:266–270, 1997.

[37] A B Nordmark. Existence of priodic orbits in grazing bifurcations of impacting mechanical oscillators. *Nonlinearity*, 14:1517–1542, 2001.

[38] H. Nusse, E. Ott, and J. Yorke. Border collision bifurcations: an explanation for observed bifurcation phenomena. *Phys. Rev. E*, 49:1073–1076, 1994.

[39] M. Oestreich, N. Hinrichs, K. Popp, and C. J. Budd. Analytical and experimental investigation of an impact oscillator. *Proceedings of the ASME 16th Biennal Conf. on Mech. Vibrations and Noise*, DETC97VIB-3907:1–11, 1997.

[40] F. Peterka. Part 1: Theoretical analysis of n-multiple $(1/n)$-impact solutions. *CSAV Acta Technica*, 19:462–473, 1974.

[41] F. Peterka. Results of analogue computer modelling of the motion. part 2. *CSAV Acta Technica*, 19:569–580, 1974.

[42] F. Pfeiffer and C. Glocker. *Multibody dynamics with unilateral constraints.* Chichester, 1996.

[43] P. T. Piiroinen, H. J. Dankowicz, and A. B. Nordmark. On a normal-formal analysis for a class of passive bipedal walkers. *International Journal of Bifurcation and Chaos*, 11(9):2411–2425, 2001.

[44] P.T. Piiroinen and H.J. Dankowicz. Low-cost control of repetetive gait in passive bipedal walkers. To apper in *International Journal of Bifurcation and Chaos*, 2003.

[45] P.T. Piiroinen, H.J. Dankowicz, and A.B. Nordmark. Breaking symmetries and constraints: Transitions from 2D to 3D in passive walkers. *Multibody System Dynamics*, 10:147–176, 2003.

[46] K. Popp and P. Shelter. Stick–slip vibrations and chaos. *Philosophical Transactions of the Royal Society A*, 332(1624):89–105, 1990.

[47] S. W. Shaw and P. J. Holmes. Periodically forced linear oscillator with impacts: chaos and long-periodic motions. *Phys. Rev. Lett.*, 51:623–626, 1983.

[48] K N Slade, L N Virgin, and P V Bayly. Extracting information from interimpact intervals in a mechanical oscillator. *Physical Review E*, 56(3):3705–3708, 1997.

[49] A. Stensson and A. Nordmark. Experimental investigation of some consequences of low velocity impacts in the chaotic dynamics of a mechanical system. *Phil. Trans. Roy. Soc. Lond A*, 347:439–448, 1994.

[50] W.J. Stronge. *Impact Mechanics*. CUP, Cambridge, 2000.

[51] J. M. T. Thompson and R. Ghaffari. Chaotic dynamics of an impact oscillator. *Phys. Rev. A*, 27:1741–1743, 1983.

[52] L. N. Virgin. *Introduction to Experimental Nonlinear Dynamics: A Case Study in Mechanical Vibration*. Cambridge University Press, Cambridge, 2000.

[53] D.J. Wagg, Karpodinis G., and Bishop S.R. An experimental study of the impulse response of a vibro-impacting cantilever beam. *J. Sound Vib,*, 228:242–264, 1999.

[54] G. S. Whiston. Global dynamics of a vibro-impacting linear oscillator. *J. Sound Vib.*, 118:395–429, 1987.

[55] G. S. Whiston. The vibro-impact response of a harmonically excited and preloaded one-dimensional linear oscillator. *J. Sound Vib.*, 115:303–324, 1987.

[56] G.S. Whiston. Singularities in vibro-impact dynamics. *J. Sound Vib.*, 152:427–460, 1992.

[57] G. Zhou and S.R. Reid, editors. *Impact on Composites*. Woodhead Publishers, 2000.